

# Increasing plastic hinge length using two pipes as web at reduced beam section, an experimental and numerical study

Seyed M. Zahrai<sup>1b</sup>, Seyed R. Mirghaderi<sup>1a</sup> and Aboozar Saleh<sup>\*2</sup>

<sup>1</sup> School of Civil Engineering, College of Engineering, The University of Tehran, Iran

<sup>2</sup> Department of Civil Engineering, Islamic Azad University Professor Hesabi Branch, Tafresh, Iran

(Received October 15, 2016, Revised January 09, 2017, Accepted January 17, 2017)

**Abstract.** Experimental and numerical studies of a newly developed Reduced Beam Section (RBS) connection, called Tubular Web RBS connection (TW-RBS) have been recently conducted. This paper presents experimental and numerical results of extending the plastic hinge length on the beam flange to increase energy dissipation of a proposed version of the TW-RBS connection with two pipes, (TW-RBS(II)), made by replacing a part of flat web with two steel tubular web at the desirable location of the beam plastic hinge. Two deep-beam specimens with two pipes are prepared and tested under cyclic loads. Obtained results reveal that the TW-RBS(II) like its type I, increases story drift capacity up to 6% in deep beam much more than that stipulated by the current seismic codes. Based on test results, the proposed TW-RBS(II) helps to dissipate imposed energy up to 30% more than that of the TW-RBS(I) specimens at the same story drift and also reduces demands at the beam-to-column connection up to 30% by increasing plastic hinge length on the beam flange. The TW-RBS(II) specimens are finally simulated using finite element method showing good agreement with experimental results.

**Keywords:** energy dissipation; plastic hinge length; reduced beam section; accordion web RBS; two pipes; accordion cells

## 1. Introduction

Reduced Beam Section (RBS) moment connection is one of the most economical and practical prequalified connections among the post-Northridge ones. RBS connection was initially proposed by intentionally reducing the plastic flexural capacity of the beam section away from the column face to induce the plastic hinge at desirable location. This feature of RBS can lead to significant reduction in the developed demands on the beam-column connection as well as its components such as panel zone, continuity plate and related welds.

Two methods of reducing the plastic moment of the beam flange have been suggested previously: cutting and drilling the flanges. SAC committee (FEMA 2000b) during 1996 to 1998 showed that the radius cut RBS connection has better behavior compared to other shapes of flange cut and the connection behavior depends on the beam depth. Conventional RBS moment connection in addition to the reduction in plastic moment capacity would also experience noticeable reduction in the out-of-plane stiffness of the beam. This latter feature can arise some concerns in terms of lateral torsional stability of the section. The reduced beam section usually experiences web local buckling first, followed by lateral torsional buckling and finally flange

local buckling (Naeim 2001). The amplitude of the lateral torsional buckling tends to be larger when the RBS is used for deep beams, giving rise to twisting in the columns. In these cases, lateral bracing around the RBS should be provided (Naeim 2001). Pachoumis *et al.* (2010) showed that use of RBS connections in European sections requires some modifications on the RBS geometric parameters. Therefore, other section reduction details have been proposed for RBS connections to resolve this matter as follows:

### a. Reducing the web height

Wilkinson *et al.* (2006) evaluated a new detail by which the web height reduction near the connection of beam-to-column was achieved. The experimental results approved a plastic rotation capacity of more than 5%.

### b. Connection with web reduction

In FEMA 350 (2000a) a new type of reduced connection has been proposed in which the demand reduction at the column face is provided through making a circular hole in the beam web close to the connection. Behavior of RBS connections with web circular holes has been investigated by Yang and Yang (2009). Behavior of beams with perforated webs has been also studied by Tsavdaridis and D'Mello (2012). They have focused on beams with elliptical web opening and concluded that such details can lead to satisfactory results both in terms of technical and constructional points of view.

\*Corresponding author, Assistant Professor,  
E-mail: [aboozar.saleh@ut.ac.ir](mailto:aboozar.saleh@ut.ac.ir)

<sup>a</sup> Professor, E-mail: [mzahrai@ut.ac.ir](mailto:mzahrai@ut.ac.ir)

<sup>b</sup> Associate Professor, E-mail: [rmirghaderi@ut.ac.ir](mailto:rmirghaderi@ut.ac.ir)

### c. Heat-treated beam section (HBS)

The technique involves reducing the strength of specified regions of the beam flanges by exposing them to high temperatures followed by slow cooling as studied by Morrison *et al.* (2015). Contrary to RBS, HBS connection does not sacrifice elastic stiffness or buckling resistance. They tested two large scale connections modified with the HBS technique leading to the promotion of yielding and plastic hinge development in the heat-treated regions with specimens attaining inter-story drifts as high as 6% without weld or near weld fracture.

### d. Combination of RBS connections

Ataollahi *et al.* (2016) studied the cyclic behavior of a new proposed connection developed by using a combination of strengthening the connection concept by T-stub connection; and weakening the beam ends concept by RBS connection. The results show that moment capacity and dissipated energy of the new proposed connection is almost the same as those computed for a T-stub connection and higher than corresponding values for an RBS connection.

### e. Connection with accordion web

Mirghaderi *et al.* (2010) discussed and evaluated connections of corrugated web reduced cross section in shallow beams. Two symmetric angles were considered in two test samples with respect to the web as corrugated sheet to execute removed web accommodation and create a cross section as accordion web RBS (AW-RBS). In this connection the flange stability condition is improved due to the smaller width-to-thickness ratio of beam flange. In this regard, no lateral-torsional buckling happens at the connection.

Experimental and numerical investigations of a new type of RBS connection, TW-RBS, have been recently proposed by the authors in deep and shallow beams (Saleh *et al.* 2016a, b) through replacing a part of flat web with a pipe at the desired location of the beam plastic hinge. The results have shown that using the TW-RBS like the AW-RBS can reduce the plastic strain demand near CJP welds, due to flexural strength reduction by replacing pipe in the TW-RBS connection. Accordingly, no fracture is observed outside the plastic hinge area and the plastic strains are effectively concentrated within the reduced region. Improving the out-of-plane stiffness about the beam longitudinal axis is the most important feature of using the pipe; also the TW-RBS provides even a better condition than AW-RBS connection in terms of low-cycle fatigue due to experimental results, by changing sharp corners of angles to arc shape of the pipe in beam section. The TW-RBS connection well satisfies the requirements of rigid connection according to AISC and FEMA up to 6% story drift.

In this paper by using two pipes next to each other at the web of deep beams, the objective is to increase the plastic hinge length on the beam flange of the TW-RBS connection to improve energy dissipation and at the same time reduce demands at the beam-to-column connection of the TW-RBS

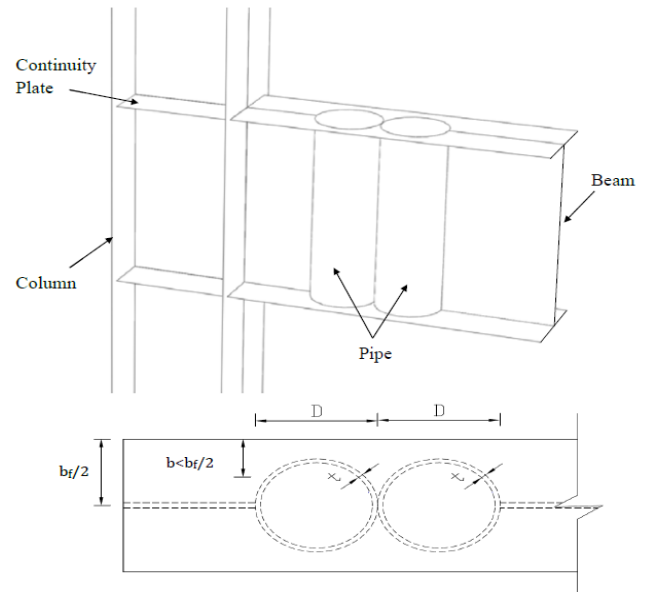


Fig. 1 Proposed connection to increase the plastic hinge length

connection. For this purpose, an experimental program including two specimens of deep beams with two accordion-cells in the TW-RBS connections under cyclic loading is presented. Experimental results are compared to those of the TW-RBS with an accordion cell (TW-RBS-I) (Saleh *et al.* 2016a). Also the connection is numerically studied for more investigation and classification.

## 2. Proposed connection to increase plastic hinge length

The configuration of the proposed connection is illustrated in Fig. 1. As shown in the figure, two pipes are used at the web of a beam with I-section in a limited zone near the column face. The beam is connected to the column face by CJP welds to develop a full capacity rigid connection. As discussed for the TW-RBS(I) (Saleh *et al.* 2016a) based on the small stiffness in the longitudinal direction in corrugated sheet, the contribution of the beam web within the corrugated region is negligible in the beam flexural strength. Therefore, a reduced section is obtained. This way the plastic zone on the beam is increased using two pipes as the tubular web. In this regard, it is expected that the stability and ductility of the beam increase compared to those for TW-RBS(I). This RBS connection is called "Tubular-Web RBS connection with two accordion web", abbreviated as "TW-RBS(II)".

## 3. Experimental program

A set of tests has been carried out to experimentally study the behavior of the TW-RBS(II) moment connections and validate the efficiency of extending plastic hinge length compared to experimental results of the TW-RBS(I) (Saleh *et al.* 2016a).

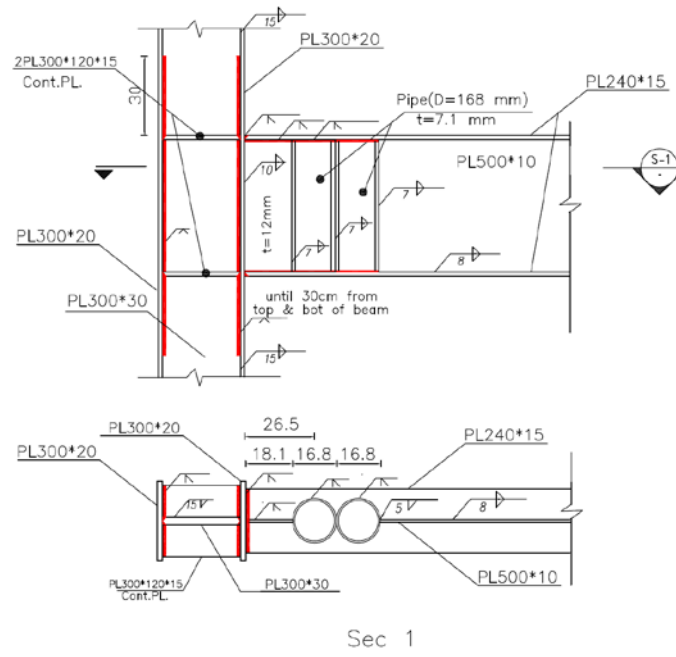


Fig. 2 TW-RBS(II) test Specimens connection details

3.1 Test specimens

In this research, two 2/3 scale identical specimens including the TW-RBS(II) connections were designed to be fabricated and tested. The specimens similar to previously tested TW-RBS(I) specimens consisted of exterior connection subassemblies with a beam attached to a column face. Also in subassembly, half of the parts of lower and upper columns were chosen as vertical elements and half of the beam was selected for horizontal element. The specimens were designed to satisfy the strong-column weak-beam criterion to ensure a plastic mechanism in the beam.

In this study, the specimens consist of built-up H column with plate of 300×30 mm<sup>2</sup> for the web and two plates of 300×20 mm<sup>2</sup> for the flange and built up beam with plate of 500×12 mm<sup>2</sup> and 500×10 mm<sup>2</sup> for the web respectively for region between pipe and column face and for region after pipe, and two plates of 240×15 mm<sup>2</sup> for the flange. The TW-RBS connections are constructed by replacing a specified length of beam web with a pipe segment. The pipe used in test specimens has outside diameter of 168 mm and thickness of 7.1 mm. The lengths chosen for column and beam are respectively 2400 mm and 2000 mm. The selected sections satisfy the width-thickness ratio of seismically compact sections.

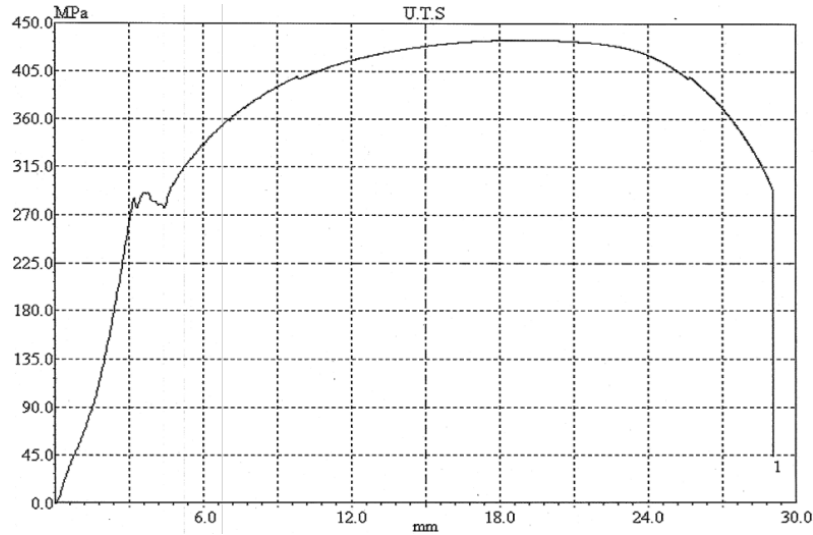
All details are like the TW-RBS(I) specimens (Saleh *et al.* 2016a), except for the thickness of beam web for region between the pipe and column face. In the TW-RBS(I), beam web at this region had thickness of 10 mm while it has increased 2 mm in this research. The reason for this is that nominal plastic flexural strength at the column face has increased and the ratio of maximum moment demand at the column face to the nominal plastic strength has decreased to 0.9 (Section 3.2) similar to the recommended value for this parameter in design of common reduced beams (Engelhardt

*et al.* 1998). The TW-RBS(II) connection details of both specimens prepared in a fabrication shop are illustrated in Fig. 2.

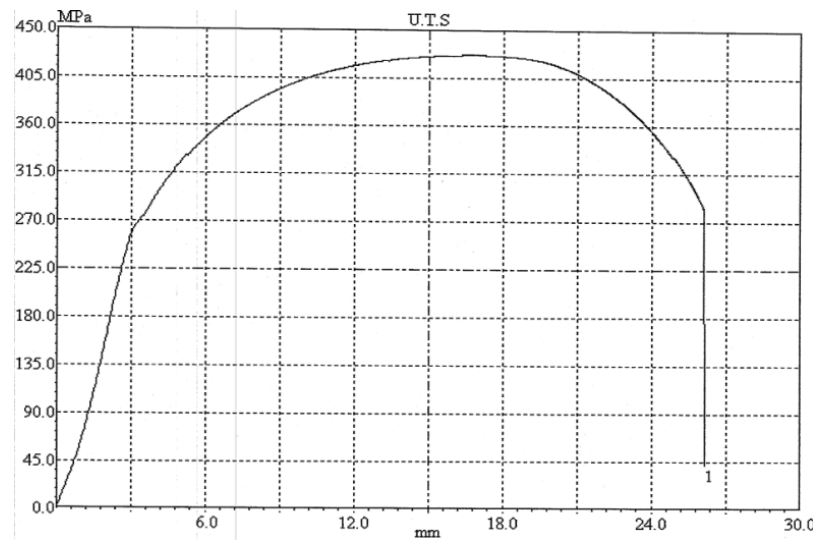
The beam flanges were connected to the column face by applying a prequalified CJP groove weld detail without backing bar with a root pass and a reinforcing fillet. CJP groove welds were applied between the continuity plates and the column flanges. Also CJP groove welds were used to connect pipes to beam flange and flat web that is at region between pipe and column face to beam flange. The connection between column web and flanges at panel zone up to 300 mm from top and bottom of the beam was also made by CJP groove welds. Other connections such as beam web to the column face, pipes to beam web and pipe to pipe were connected by fillet welding. All groove welds were ultrasonically checked and all fillet welds were visually tested by a licensed inspector. The beams, columns, continuity plates and corrugated plates were all of A36 steel with nominal yield stress of 240 MPa. The mechanical properties of steel coupons, obtained from the specimens, are presented in Table 1, in accordance with ASTM A370 standard for tensile testing of the steel. The stress-

Table 1 Mechanical properties of steel coupons taken from different components of test subassembly

| Test specimen | Member | Coupon | Yield strength (MPa) | Tensile strength (MPa) | Elongation (%) |
|---------------|--------|--------|----------------------|------------------------|----------------|
| 1 & 2         | Beam   | Web    | 291                  | 435                    | 40.5           |
| 1 & 2         | Beam   | Flange | 273                  | 427                    | 40.0           |
| 1 & 2         | Column | Web    | 261                  | 417                    | 44.0           |
| 1 & 2         | Column | Flange | 256                  | 425                    | 44.0           |
| 1 & 2         | Pipe   | -      | 344                  | 491                    | 29.0           |



(a) Beam web coupon



(b) Beam flange coupon

Fig. 3 The stress-elongation curves for beam flat web and flange coupons

Table 2 Beam design control at the column face

| $Z_{TW-RBS}$<br>( $m^3 \times 10^{-6}$ ) | $M_{TW-RBS}$<br>(kN-m) | $L$<br>( $m \times 10^{-2}$ ) | $E$<br>( $m \times 10^{-2}$ ) | $M_f$<br>(kN-m) | $Z_b F_{ye}$<br>(kN-m) | $\alpha$ | $e + d_c/2$<br>( $m \times 10^{-2}$ ) | $\sum M_{pb}$<br>(kN-m) | $\sum M_{pc}$<br>(kN-m) | $\sum M_{pc} / \sum M_{pb}$ |
|--|------------------------|-------------------------------|-------------------------------|-----------------|------------------------|----------|---------------------------------------|-------------------------|-------------------------|-----------------------------|
| 1891.5                                   | 649.1                  | 196.5                         | 26.5                          | 736.6           | 812.4                  | 0.907    | 43.5                                  | 792.8                   | 1472.0                  | 1.85                        |

$$\text{Plastic section modulus of the TW-RBS: } Z_{TW-RBS} = Z_{\text{flange}} + \left(1 - \frac{2\left(\frac{t_c}{t_f}\right)}{\left(\frac{D}{t_f}\right)}\right) Z_{\text{web}}^{\text{flat}}$$

Thickness of pipe:  $t_c$ ; Diameter of pipe:  $D$ ; Thickness of flat web:  $t_f$

Expected moment in plastic hinge location:  $M_{TW-RBS} = 1.1R_y Z_{TW-RBS} F_y$

Distance between the centerline of nearest pipe to column to middle span:  $L$

Distance between the centerline of nearest pipe to column to the column face:  $e$

Beam moment at the column face location:  $M_f = M_{TW-RBS} (II) \frac{(L+e)}{L}$

Plastic modulus in unreduced beam and column sections:  $Z_b$  and  $Z_c$

Moment ratio at the column face:  $\alpha = \frac{M_f}{Z_b F_{ye}}$ , Column depth:  $d_c$

Beam moment in center of column:  $\sum M_{pb} = M_f$ ; Column plastic moment:  $\sum M_{pc} = \sum Z_c F_{yc}$

Table 3 Local and general buckling strength of pipes

| $d$<br>( $m \times 10^{-2}$ ) | $a$<br>( $m \times 10^{-2}$ ) | $b$<br>( $m \times 10^{-2}$ ) | $c$<br>( $m \times 10^{-2}$ ) | $\omega$<br>( $m \times 10^{-2}$ ) | $t_w$<br>( $m \times 10^{-2}$ ) | $h_w$<br>( $m \times 10^{-2}$ ) | $\eta$ | $k_l$ | $\tau_{cr,l}^e$<br>(MPa) | $k_G$ | $\tau_{cr,G}^e$<br>(MPa) |
|-------------------------------|-------------------------------|-------------------------------|-------------------------------|------------------------------------|---------------------------------|---------------------------------|--------|-------|--------------------------|-------|--------------------------|
| 16.8                          | 16.8                          | 0.0                           | 16.8                          | 16.8                               | 0.71                            | 50                              | 0.5    | 5.79  | 1897.3                   | 931.6 | 34465                    |

Depth, Thickness and Height of pipe:  $d$ ,  $t_w$  and  $h_w$

Horizontal width, horizontal image of diagonal width and diagonal width of corrugated sheet:  $a$ ,  $b$  and  $c$

Maximum value of horizontal width and diagonal width of corrugated sheet:  $\omega = \max(a, c)$

Length reduction factor:  $\eta = (a + b) / (a + c)$  local shear buckling coefficient:  $k_l = 5.34 + 4 \left(\frac{\omega}{h_w}\right)^2$

Elastic local buckling shear stress:  $\tau_{cr,l}^e = k_l \frac{\pi^2 E}{12(1-\nu^2)} \left(\frac{t_w}{\omega}\right)^2$ ; General shear buckling coefficient:  $k_G = \frac{36\beta}{\pi^2 \sqrt{\eta}} \left[ 2 \left(\left(\frac{d}{t_w}\right)^2 + 1\right) (1 - \nu^2) \right]^{3/4}$

Global buckling of corrugated sheet:  $\tau_{cr,G}^e = k_G \frac{\pi^2 E}{12(1-\nu^2)} \left(\frac{t_w}{h_w}\right)^2$

elongation curves for beam flat web and flange coupons are shown in Fig. 3.

### 3.2 Design procedure of the TW-RBS(II) connection

The TW-RBS(II) connection is designed as the TW-RBS(I) connection (Saleh *et al.* 2016a). It should be noted that in the TW-RBS(II), the closer pipe to column due to its greater demand, is taken as basic reduced section used in design. In this study, overview of the design procedure is given.

The expected moment is specified in the beam plastic hinge location of the TW-RBS(II) specimens and the condition of weak beam-strong column is provided, as presented in Table 2. The expected yield stress ( $F_{ye}$ ) was calculated based on a nominal yield stress of 240 MPa and  $R_y$  factor of 1.3. Sufficient safety factor for column face demand is provided ( $\alpha = 0.907$ ).

As mentioned in the TW-RBS(I) (Saleh *et al.* 2016a), in corrugated sheets, shear buckling is controlled by interaction of buckling mode obtained from interaction of local and global buckling modes. The local and general buckling strengths of pipes are presented in Table 3 where expected yielding stress of material is used.

The equation for interaction shear buckling strength can be used for unusual corrugated sheets such as arcs (Eldib 2004). Calculated results for shear control are provided in Table 4 using yielding stress of material. Furthermore,  $\Phi_v = 0.9$  and yield shear stress of  $\tau_y = 0.577F_y = 138.5$  MPa are considered.

### 3.3 Test setup and instrumentation

For this study, the tests were conducted in the structural

laboratory of the Building and Housing Research Center of Iran. The test setup was designed to provide expected boundary conditions for the subassemblies. The column base was fixed to the strong floor by a pin connection and the beam end was supported with lateral movement capability to provide the roller boundary condition. A hydraulic actuator with 500 kN capacity and 250 mm stroke was used to apply cyclic horizontal displacements to the top end of the column. The lateral supports were provided by applying two external frames for each beam and another one near the loading point for the column in order to avoid out-of-plane movement of the specimen, lateral-torsional buckling of beams, column rotation, and local instabilities at the loading point. The test setup configuration and overall dimensions of the specimens are similar to Part 1 (Saleh *et al.* 2016a), as shown in Fig. 4.



Fig. 4 Test setup configuration and overall dimensions of the specimens

Table 4 Shear control of flat and tubular web

| $\tau_{cr}$<br>(MPa) | $t_w$<br>( $m \times 10^{-2}$ ) | $h_w$<br>( $m \times 10^{-2}$ ) | $V_{nt}$<br>(kN) | $t_{wf}$<br>( $m \times 10^{-2}$ ) | $d_b$<br>( $m \times 10^{-2}$ ) | $V_{nf}$<br>(kN) | $V_g$<br>( $m \times 10^{-2}$ ) | $V_u$<br>(kN) | $V_f$<br>(kN) | $V_u / \Phi_v V_{nt}$ | $V_f / \Phi_v V_{nf}$ |
|----------------------|---------------------------------|---------------------------------|------------------|------------------------------------|---------------------------------|------------------|---------------------------------|---------------|---------------|-----------------------|-----------------------|
| 87.2                 | 0.71                            | 50                              | 619.1            | 1.0                                | 50                              | 720              | 0.0                             | 330.3         | 374.8         | 0.59                  | 0.58                  |

$$\left(\frac{1}{\tau_{cr,l}^e}\right)^{1.5} = \left(\frac{1}{\tau_{cr,G}^e}\right)^{1.5} + \left(\frac{1}{\tau_y}\right)^{1.5}, \text{ global resistance calculated over yielding shear limit, then: } \tau_{cr} = \frac{\tau_y}{\sqrt[3]{2^2}} = 87.2 \text{ MPa}$$

Shear capacity of pipe:  $V_{nt} = 2 \tau_{cr} t_w h_w$ ; Flat web thickness and depth of beam:  $t_{wf}$  and  $d_b$

Shear capacity of flat web:  $V_{nf} = 0.6 F_y t_{wf} d_b$ ; Shear in plastic hinge:  $V_u = M_{TW-RBS} / L$ ; Gravity shear:  $V_g$

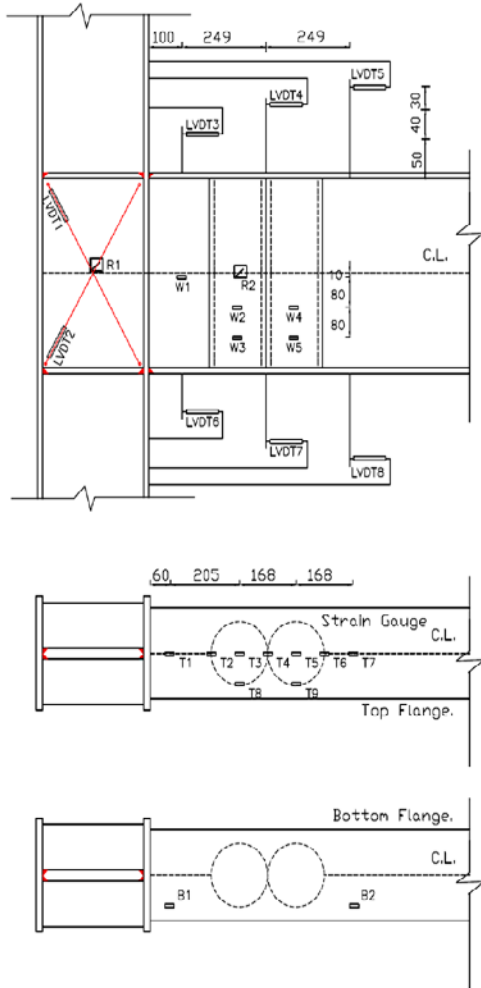


Fig. 5 The location of used strain gages and the LVDTs installed on the specimens (all dimensions are in mm)

In this research, the specimens were tested by imposing a prescribed quasi-static cyclic displacement specified in the AISC seismic provision (AISC 2010). The total story drift angle was calculated by dividing the exerted displacement by the column height. The loading history cycles consisted of six cycles at 0.375%, 0.5% and 0.75% of total story drift angle, sequentially. The next four were at 1% story drift, followed by two cycles each of successively increasing drift percentages (i.e., 2, 3, 4%, etc.). The cyclic tests were accomplished with a low rate for best monitoring the response of the specimens as well as their deformations during the loading history.

Each specimen was equipped with LVDTs and strain gages. Six LVDTs were used to monitor the plastic hinge rotation and two other diagonal ones for recording panel zone shear deformations. Several strain gages were pasted on the beam flange, beam web, pipes and panel zone in order to measure the history of strains in the specimens. The instrumentation scheme is shown in Fig. 5. The horizontal displacement of the actuator was measured by an external LVDT. The applied loads were measured by the load cell installed at back of the actuator. The data sent from the LVDTs and the strain gages were recorded using a digital data logger.

**4. The experimental results of the TW-RBS(II)**

Cyclic behaviors of the specimens are presented herein by means of test observations and also analyses of instrumentation records.

**4.1 Test observations**

**4.1.1 Observations of test specimen 1**

The first yielding of Test Specimen 1 emerged after

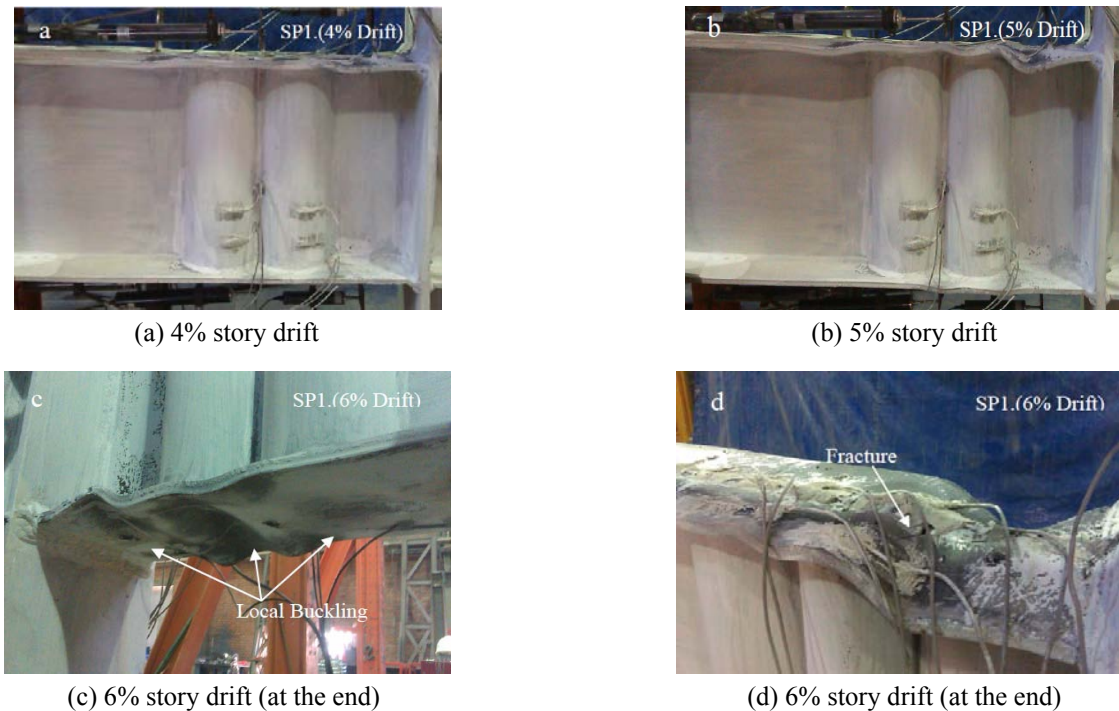


Fig. 6 Test specimen 1 and plastic hinge length extension in the beam

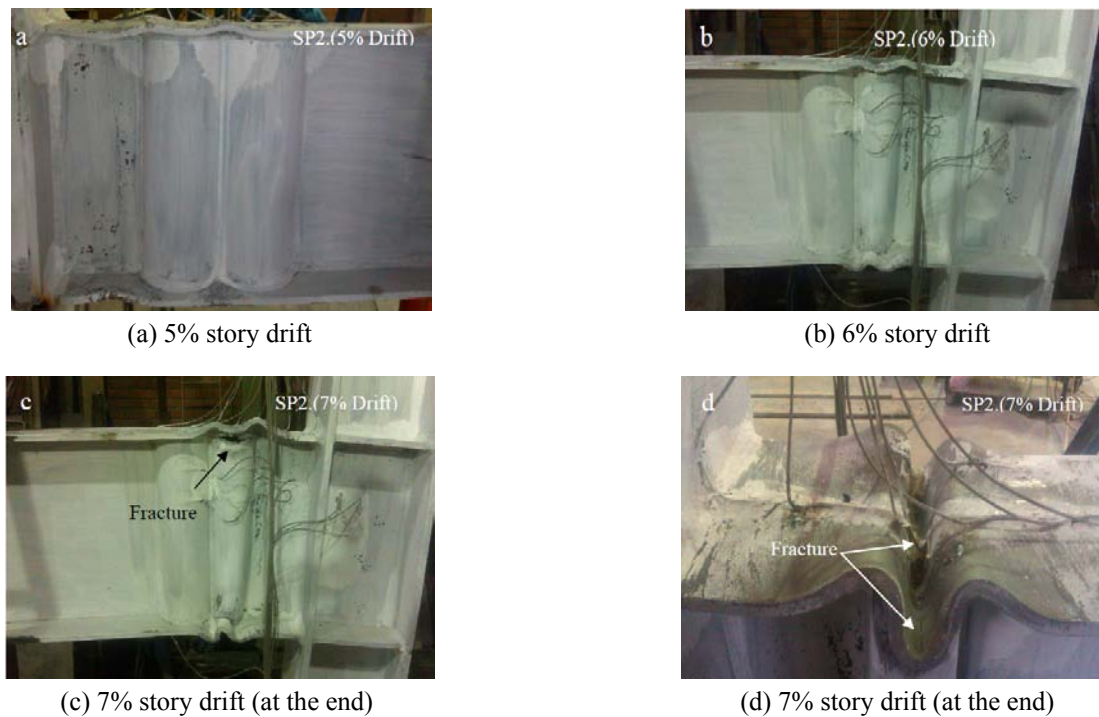


Fig. 7 Test specimen 2 and plastic hinge length extension in the beam

minor flaking of the whitewash coating of beam top flange at the center of the reduced region at closer pipe to column face during the first cycle of 1% story drift cycles. The yielding of beam flanges became more apparent around the first pipe after 1.5% story drift cycles and also appeared at beam top flange around the second pipe in this story drift. It was spread over the entire reduced region at two pipes during 2% story drift. Also flaking of the whitewash coating at the corners of flat web and at the top of the pipe web at connection region to flat web was observed. The flange yielding was extended toward the column face and beam end during the 3% story drift; minor flaking of the whitewash was observed at the bottom of connection of the pipes to each other. The yielding patterns continued during the 4% story drift cycle. Flange local buckling was detected before and in the both reduced region by two pipes on the both sides of beam and after the reduced regions on the top of beam as shown in Fig. 6(a).

In the cycles of 5% story drift, the yielding was more extended to both sides of the reduced regions and it became nearly apparent outside the reduced regions, near the column face. In addition, the amplitude of flange local buckling increased especially at the reduced region by the first pipe and also at the region close to the column face as shown in Fig. 6(b) where yielding at the pipes extended into the beam depth and the yielding at the flat web extended into the beam depth and length. Due to increasing flange local buckling and reducing the demand on the second pipe, the accordion behavior of the second pipe is accordingly reduced and not much visible.

The amplitude of buckling increased in the first half of the first cycle of 6% story drift as shown in Fig. 6(c), and the cracks were initiated in the top corner of connection of the first pipe to flat web. The cracks progressed during the

second half of the first cycle of 6% story drift. Finally, the test was terminated due to the fractures in the top flange of beam in front of reduced regions, as shown in Fig. 6(d).

#### 4.1.2 Observations of test specimen 2

During the first cycle of 1% story drift, the yielding initiated in the beam top flange at the center of the reduced region by the first pipe (closer one to column face) after a minor flaking within the reduced region. The yielding emerged at beam top flange around the second pipe at 1.5% story drift and spread over the entire reduced region by two pipes extending the plastic hinge length at the end of 2% story drift. Also flaking of the whitewash coating at the corners of flat web and at the pipes at connection to flange occurred in this story drift. During the 3% story drift cycles, minor flaking was observed near CJP welds and at the bottom of connection of the pipes as well. During 4% story drift, the yielding patterns continued and flange local buckling appeared before and in reduced regions in the both sides of beam as shown in Fig. 7(a).

At the first cycle of 5% story drift the amplitudes of the flange buckling became more extensive at the reduced region by the first pipe and also at the region close to the column face as shown in Fig. 7(b). The yielding extended into the beam depth at the pipes while it extended into the beam depth and length at the flat web. At 6% story drift, the amplitude of buckling increased more at mentioned region and crushing web was observed at the first pipe near the compressive flange. In the first half of first cycle of 7% story drift, fracture was initiated at the middle of connection of first pipe to top flange as shown in Fig. 7(c). Then in the second half of first cycle of 7% story drift, the flange buckling in the reduced region by first pipe grew rapidly and a crack was appeared in this region. Finally, the test

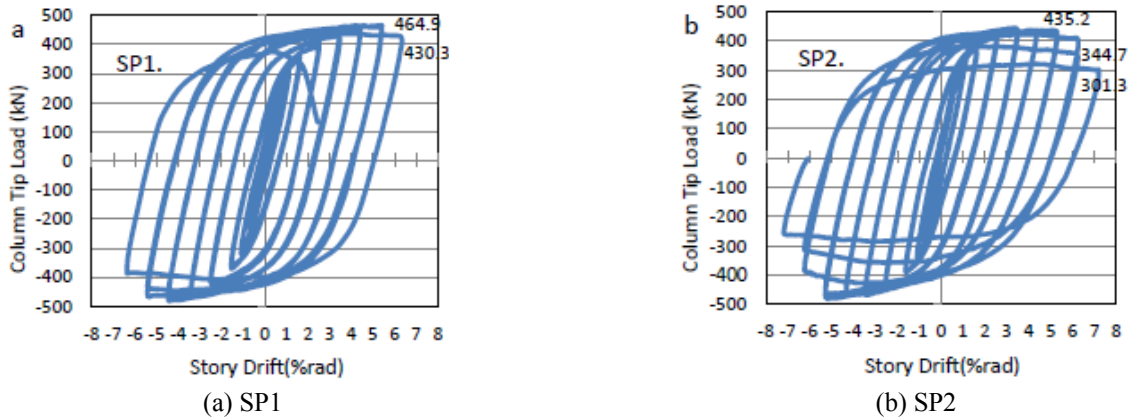


Fig. 8 Hysteretic curves for the test specimens of TW-RBS(II)

was terminated as shown in Fig. 7(d).

4.2 Investigation of the general behavior

The hysteretic curves (column tip load versus total story drift) of both specimens of the TW-RBS(II) are shown in Figs. 8(a) and (b). The total story drift was calculated by dividing the column tip displacement by the distance from the column base to the centerline of the actuator. Both specimens showed quite stable inelastic behavior and favorable energy dissipation capacity due to plastic hinge length extension. According to AISC seismic (2010)

acceptance criteria, the flexural capacity of the specimen at the column face should not be less than 80% of the beam plastic moment until 4% story drift to confirm the connection. The results of the proposed connection well satisfy this condition as shown in Fig. 8, where until 6% story drift both specimens do not experience degradation more than 20% of the beam plastic moment.

The TW-RBS(II) also met FEMA350 criteria as the test specimens adequately resisted. The mentioned criteria require achieving a total rotation story drift of 4% before the maximum of 20% strength degradation or crack happening in the connection and a 6% story drift before losing the total resistance. The crack occurred in the TW-RBS(II) connection at 0.06 and 0.07 rad respectively for SP1 and SP2.

The moment at the column face of the beam versus rotation, of the specimen 1 is shown in Fig. 9. The rotation was obtained by dividing horizontal displacement difference of LVDT 5 and 8 (Fig. 5) by their vertical distance ( $\theta = \Delta L/H$ ). This rotation is the plastic rotation of beam inclusive of the elastic rotation of the column face and also before the plastic zone.

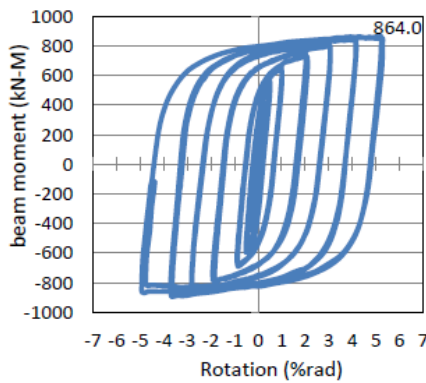


Fig. 9 Hysteretic curves of the moment - rotation for the specimen 1

4.3 Investigation of the plastic hinge behavior

The strain envelope of top flange in a longitudinal section of beam has been illustrated in Fig. 10 where the concentration of strain appears on the center of reduced

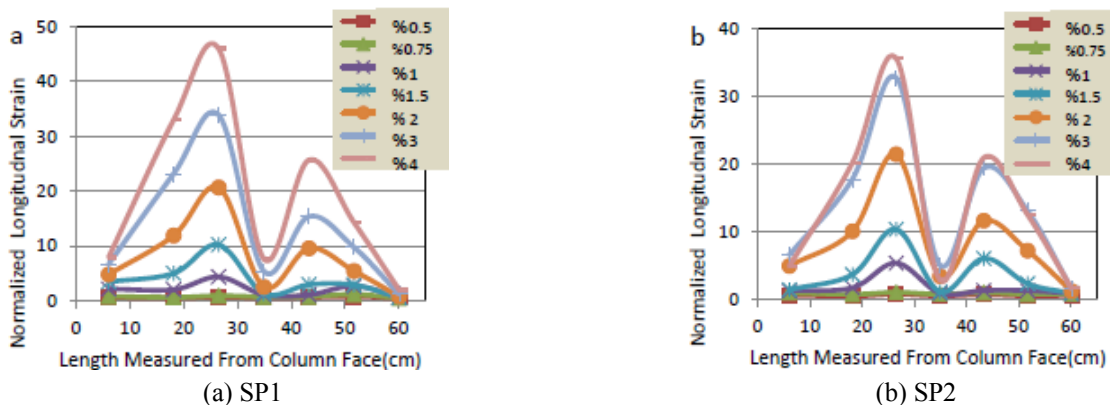


Fig. 10 Normalized longitudinal strain profile along the beam top flange

Table 5 The energy dissipation at each cyclic in the TW-RBS(II) and the TW-RBS(I) specimens

| Story drift | Energy dissipation (ED) (kN-m) |        |           |       |
|-------------|--------------------------------|--------|-----------|-------|
|             | TW-RBS(II)                     |        | TW-RBS(I) |       |
|             | SP1                            | SP2    | SP1       | SP2   |
| %1.5        | 9.37                           | 9.70   | 4.53      | 4.25  |
| %2          | 17.75                          | 19.19  | 9.18      | 10.24 |
| %3          | 40.02                          | 44.38  | 26.18     | 28.24 |
| %4          | 64.11                          | 71.59  | 47.77     | 46.25 |
| %5          | 92.85                          | 98.77  | 71.60     | 68.83 |
| %6          | 122.79                         | 131.84 | 98.05     | -     |

section along two pipes confirming the formation of the plastic hinge in the predefined regions, with higher strain values at the center of the closer pipe to the column. Evaluating the values presented in the curve shows that flange strains in the reduced section zones for the first and second pipe zones are over respectively three and two times the strains near the column face. Then the concentration of plastic strains within the reduced regions with extended plastic hinge length compared to those of TW-RBS(I) decreased the possibility of fracture at the beam-to-column CJP welds.

## 5. Verification test and result comparison

The TW-RBS with one pipe (TW-RBS(I)) is used here as benchmark and behavior validation of the TW-RBS(II) connection samples. As mentioned in Section 3.1, details of subassembly and connection of the TW-RBS(II) are the same as the TW-RBS(I) specimens. They were in turn compared to conventional RBS test previously (Saleh *et al.* 2016a).

In Fig. 11 the diagrams of column tip load versus story drift and moment versus rotation of the beam in SP1 of the TW-RBS(II) and SP2 of the TW-RBS(I) are provided. According to this figure, the cyclic performance features of the TW-RBS(II) such as stiffness and resistance in cyclic curves is the same as the TW-RBS(I) such that both connections have stable behavior up to 6% story drifts. According to Fig. 11(b), the TW-RBS(I) moment-rotation diagram is inside that of the TW-RBS(II) diagram, showing

that the ductility of the hysteretic curves at the TW-RBS(II) increase compared to the TW-RBS(I) because inelastic rotation of the beam increases due to extending plastic hinge length using two adjacent pipes as the tubular web.

To calculate the energy dissipation at each cycle, Eq. (1) is used. In this equation,  $V_y$  and  $\Delta_y$  are column tip load and displacement at the beginning of the plastic behavior of the subassembly (at 1% story drift) and  $V_i$  and  $\Delta_i$  are column tip load and displacement at the  $i$ % story drift.

$$E_D = 4(V_y\Delta_i - V_i\Delta_y) \quad (1)$$

The energy dissipation at each cycle in the TW-RBS(II) and the TW-RBS(I) specimens are presented in Table 5. In the TW-RBS(II) specimens, the energy dissipation is more up to 30% more at the same story drift. Thus, the TW-RBS(II) helps to dissipate imposed energy better by increasing plastic hinge length using two pipes next to each other as the tubular web.

In Fig. 12, normalized strains ( $\epsilon/\epsilon_y$ ) at different story drifts are presented for the specimen 1 of the TW-RBS(II) compared to these of the TW-RBS(I) specimen. Given that both samples of same connection have same results, the results of a sample in this section are used for comparison. In the diagrams, five strain categories can be recognized for the TW-RBS(II). First it presents beam flange strain at the center of reduced section at the first pipe (T3) having high strains and showing concentration of plastic strains in this zone. This part has same behavior with the center of reduced section (T3) in the TW-RBS(I) but as evident in Fig. 12, the TW-RBS(II) has lower strain level than the TW-RBS(I). The next category is strain of beam flange around reduced section at the first pipe (T2, T8) and the center of reduced section at the second pipe (T5) which has a high strain level but still experiences lower strain in comparison with center of reduced zone at the first pipe. This part has the same behavior as the region around reduced section (T2, T4, T6) in the TW-RBS(I).

The third category contains strain of beam flange around reduced section at the second pipe (T6, T9) having significant strain level but less compared to two other categories. The fourth category contains strain of beam flange in farther zones from the reduced section such as near the connection to column and the region after reduced zones (T1, T5, B1, B2) and beam flange at the contact of

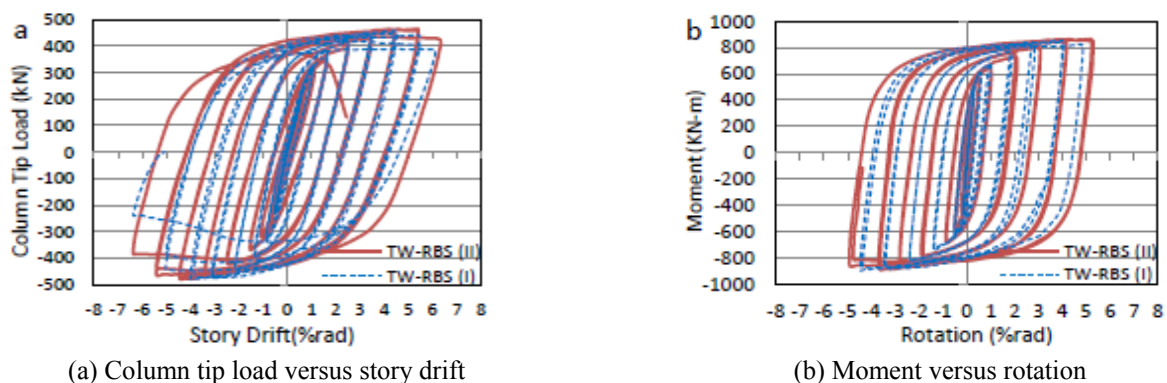


Fig. 11 Comparing the experimental cyclic responses of the TW-RBS(II) specimen to the TW-RBS(I) specimen

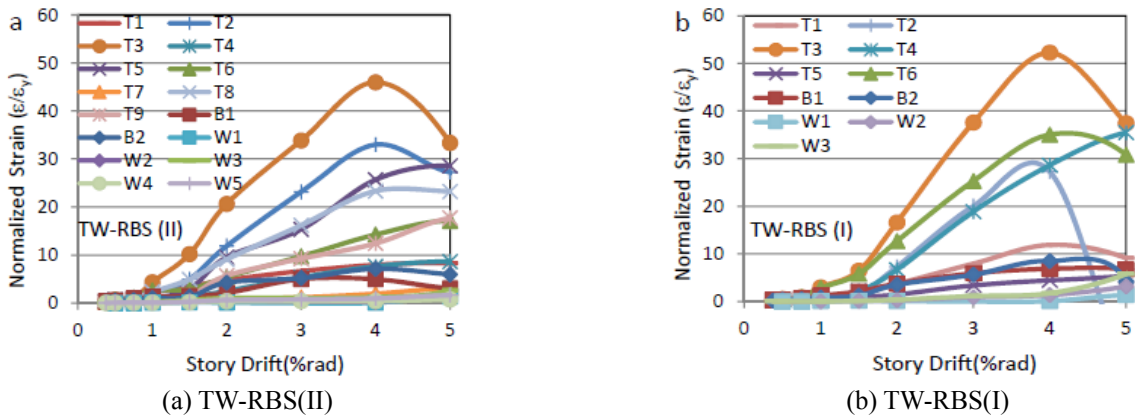


Fig. 12 Normalized strain profile at different strain gages

the two pipes (T4) with less strain level compared to three other categories. Except for T4, other points have the same behavior as the TW-RBS(I) but with lower strain level. The last category contains points on the pipes (W1, W2, W3, W4, W5) showing the lowest strain level as expected having efficient match with design theories based on accordion tubular web, same as W1, W2, W3 at the TW-RBS(I). These results show that plastic hinge in the TW-RBS(II) occurred in beam flange at pipe zones with focus respectively at center of the first and second pipe. Also based on the results, the TW-RBS(II) has extended plastic strain zone due to plastic hinge length increase with less strain level than the TW-RBS(I).

In Fig. 13, normalized strains ( $\epsilon/\epsilon_y$ ) at the width of beam flange at different distances from the column face, such as near column face (6 cm from column face), the center of reduced section by first pipe (26.5 cm from column face) and the center of reduced section by second pipe (43.3 cm from column face) at 4% story drift are presented for the specimen 1 of the TW-RBS(II). These locations for the TW-RBS(I) are near column face (10 cm from column face) and the center of reduced section (26.5 cm from column face). The comparison of results shows that although the measured strain region at the TW-RBS(II) is closer to column face to the TW-RBS(I) (6 cm to 10 cm), strains at the TW-RBS(II) are less than the TW-RBS(I) by up to 30%. Then the second pipe expands the plastic zone during the

length of the beam flange and reduces the strain level at various points such as near the connection of beam to column and improves the behavior of the TW-RBS connections.

In Fig. 14 beam axial behavior is presented at different story drift. The measure of decrease or increase of the beam length is calculated by sum of the result of LVDT 5 and 8, divided by 2. Fig. 14 shows that the TW-RBS connections have length increase at initial story drift because accordion

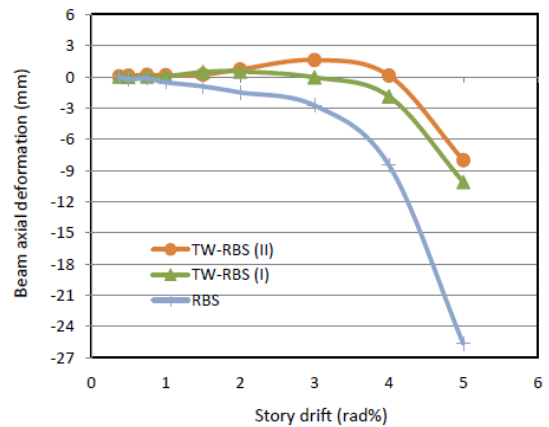


Fig. 14 Comparison of beam axial deformation at different story drifts

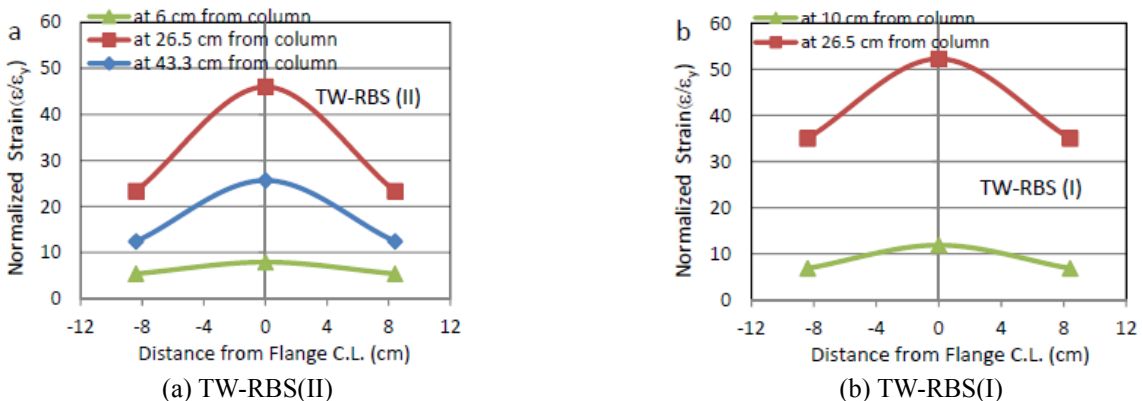


Fig. 13 Normalized strain profile at the width of beam flange at different distances from the column face at 4% story drift

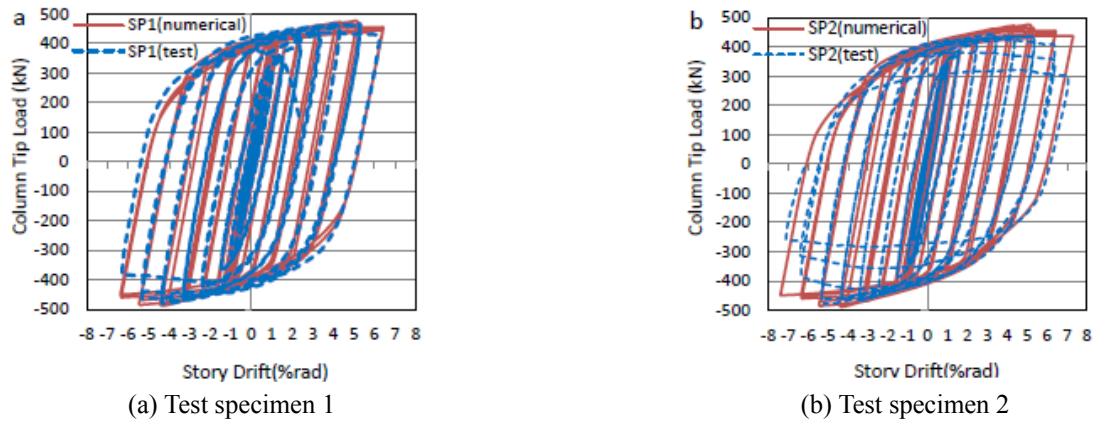


Fig. 15 Comparing the experimental cyclic responses to the finite element cyclic results of TW-RBS(II)

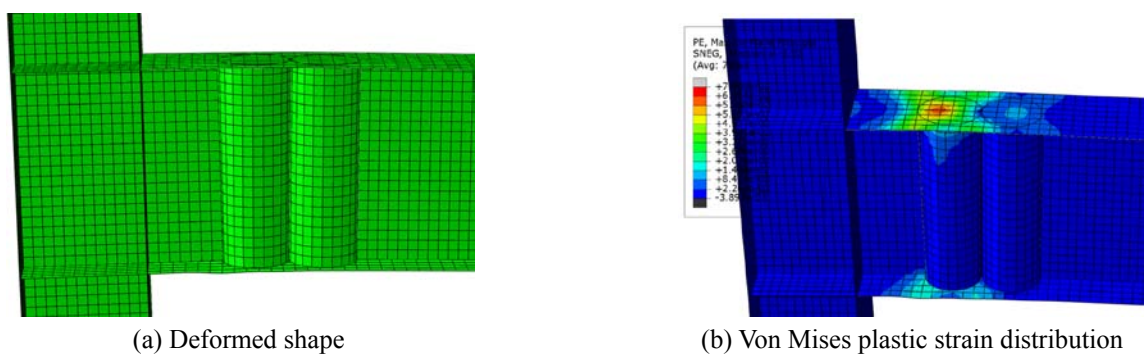


Fig. 16 Numerical results at 4% story drift

behavior of the beam web of the TW-RBS connections leads to this behavior. From 4% story drift, the local buckling is observed in the TW-RBS connections and the beam shows some length decrease. Using two pipes as the tubular web in the TW-RBS(II) creates a decrease in the axial deformation demand of specimens in which change of the beam length is less than that of the TW-RBS(I) at the end. In conventional RBS connection, the beam length decreases from the beginning. Decrease of axial deformation makes better condition for the beam to column connection.

## 6. Numerical study of the TW-RBS(II) behavior

The connection cyclic behavior has been investigated numerically after being calibrated by the experimental results for better understanding of the cyclic behavior of the TW-RBS(II) connection.

### 6.1 Finite element modeling and analysis

Numerical analysis is carried out using a three-dimensional finite element model in ABAQUS (1997). The geometry of finite element models, including member section sizes and all dimension and boundary conditions, are considered as per the subassembly used in the experimental program same as the TW-RBS(I). Given the assumption of the SHELL behavior of components in this model, deformable SHELL is defined for all components.

Four-node tetrahedral element with six degrees of freedom is used for meshing the components. Mesh size of all components is similar (maximum dimension 2.5 cm) except for beam flange in which larger mesh size is considered (maximum dimension 3 cm). All regarded elements are square-shaped and degrees of freedom in connection zone are bound together with Tie constraints. The kinematic hardening was selected for plastic properties, the yield for beam flange in which larger mesh size is considered strength ( $F_y$ ) and the ultimate strength ( $F_u$ ) and also the plastic strain of the materials are considered as per the tensile coupon test results, as summarized in Table 1. The Young modulus of elasticity and Poisson ratio are assumed as 203 GPa and 0.3, respectively, for all materials of the analysis. The standard solver of ABAQUS software (ABAQUS/Standard) was used for analyzing the model. In load section, supports were defined by setting up boundary conditions. Furthermore, cyclic loading was imposed on the numerical model by defining boundary conditions as a displacement on column tip based on AISC Seismic Provisions (2010), similar to the experimental loading protocol. Boundary condition for bottom of the column was defined by fixing degree of freedom in 3 directions. Roller support was defined for the beam at 223 cm from the column face by fixing degree of freedom in vertical direction. To define lateral support, out-of-plane displacement of the beam web was fixed at 117 and 177 cm from central of the column. Also the column was fixed with a lateral support in its upper half at 70 cm from central of the column.

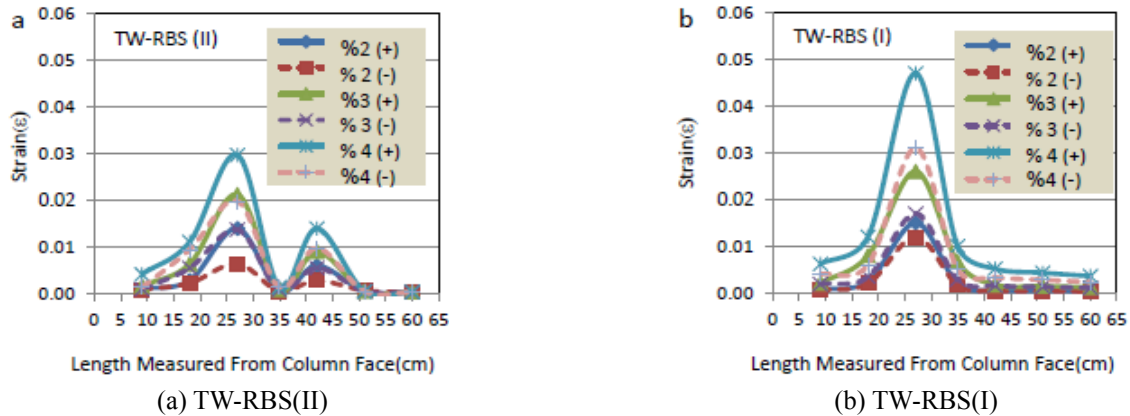


Fig. 17 Longitudinal strain profile along the beam top and bottom flange at numerical study

## 6.2 Numerical results

The numerical cyclic responses of the specimens are correlated suitably by experimental results of both specimens of the TW-RBS(II), as shown in Fig. 15. Therefore, column tip force versus story drift cyclic curves of the finite element models used in this study are confirmed in predicting the cyclic behavior of the connection. The drift is obtained from dividing lateral displacement at column tip to the column height.

The deformed shape and the plastic strain distribution are shown at 4% story drift in Fig. 16. The results show that two plastic hinges are formed at the flange in the centers of pipe areas. The beam flange around the first pipe for having a greater force demand shows the higher strain level than that around the second pipe as shown in Fig. 16(b). The second pipe increases plastic hinge length and causes the plastic strain in the surrounding pipe areas to have far less intensity while the rest of area remains elastic. This reduction in strain demand at the column face in the beam-to-column connection significantly reduces the risk of the failure at the CJP welds.

Longitudinal strain profiles along the beam tensile and compressive flanges are shown at different story drift in Fig. 17 by numerical study for both the TW-RBS(II) and the TW-RBS(I) models. According to the figure and same as experimental results, the TW-RBS(II) models using the second pipe expand the plastic zone along the length of the beam flange and reduce the strain level at various points such as near the connection of beam to column improving the behavior of the TW-RBS connections.

## 7. Conclusions

The Tubular Web RBS connection is made by replacing a part of flat web with a pipe at the desired location of the beam plastic hinge. In the TW-RBS connection due to flexural strength reduction by replacing a web strip with a pipe, the plastic strains are effectively concentrated within the reduced region at beam flange around the pipe while the plastic strain demand near CJP welds is reduced. This paper presents experimental and numerical results of the TW-RBS connection with two tubular webs called TW-RBS(II) with

the aim of extending the plastic hinge length on the beam flange and thus increasing energy dissipation. The experimental results demonstrated that the TW-RBS(II) like the TW-RBS(I) provides excellent ductility up to 6% story drift without significantly reducing the bending strength at the column face while no fracture is observed outside the plastic hinge area in the tests. Therefore, the proposed connection satisfies the requirements of rigid connection according to AISC and FEMA. In addition, the following are concluded as per the presented experimental and numerical results:

- The TW-RBS(II) extends plastic hinge length at the beam flange using two pipes as the accordion web and increases energy dissipation up to 30% compared to the TW-RBS(I) at the same story drift.
- The TW-RBS(II) reduces demand at the beam-to-column connection and also at the other points up to 30%. Then the TW-RBS(II) further improves seismic performance of this kind of connection compared to the TW-RBS(I).
- The TW-RBS(II) makes better condition in the axial deformation compared to the TW-RBS(I) by reducing the axial deformation demand.

## Acknowledgments

Authors would like to thank Islamic Azad University Professor Hesabi Branch for supporting this research project and the BHRC (Building and Housing Research Center) of Iran for conducting the experimental work. Their assistance is highly appreciated.

## References

- ABAQUS/PRE (1997), User's manual, Hibbit, Karlsson and Sorensen Inc.
- American Institute of Steel Construction (AISC) (2010), Seismic Provisions for Structural Steel Buildings, Chicago, IL, USA.
- Ataollahi, S., Banan, M.R. and Banan, M.R. (2016), "Numerical cyclic behavior of T-RBS: A new steel moment connection", *Steel Compos. Struct., Int. J.*, **21**(6), 1251-1264
- Eldib, M.E. (2004), "Buckling analysis of beams with corrugated

- webs”, *Proceeding of 5th International Conference on Civil and Architecture Engineering (ICCAE Conf)*, Singapore, May.
- Engelhardt, M., Winneberger, T., Zekany, A. and Potyraj, T. (1998), “Experimental investigation of Dog bone moment connections”, *Eng. J. AISC*, Fourth Quarter, 128-139.
- Federal Emergency Management Agency (2000a), FEMA-350, Seismic design criteria for new moment resisting steel frame construction, Washington, D.C., USA.
- Federal Emergency Management Agency (2000b), FEMA-355D, State of the art report on connection performance, Washington, D.C., USA.
- Mirghaderi, S.R., Torabian, S. and Imanpour, A. (2010), “Seismic performance of the accordion-web RBS connection”, *J. Constr. Steel Res.*, **66**, 277-288.
- Morrison, M., Schweizer, D. and Hassan, T. (2015), “An innovative seismic performance enhancement technique for steel building moment resisting connections”, *J. Constr. Steel Res.*, **109**, 34-46.
- Naeim, F. (2001), *The Seismic Design Handbook*, (2nd Ed.), Kluwer Academic Publishers, 418 p.
- Pachoumis, D.T., Galoussis, E.G., Kalfas, C.N. and Efthimiou, I.Z. (2010), “Cyclic performance of steel moment-resisting connections with reduced beam sections-experimental analysis and finite element model simulation”, *Eng. Struct.*, **32**(9), 2683-2692.
- Saleh, A., Mirghaderi, S.R. and Zahrai, S.M. (2016a), “Cyclic testing of tubular web RBS connections in deep beams”, *J. Constr. Steel Res.*, **117**, 214-226.
- Saleh, A., Zahrai, S.M. and Mirghaderi, S.R. (2016b), “Experimental study on innovative tubular web RBS connections in steel MRFs with typical shallow beams”, *Struct. Eng. Mech., Int. J.*, **57**(5), 785-808.
- Tsavdaridis, K.D. and D’Mello, C. (2012), “Optimisation of novel elliptically-based web opening shapes of perforated steel beams”, *J. Constr. Steel Res.*, **76**, 39-53.
- Wilkinson, S., Hurdman, G. and Crouther, A. (2006), “A moment resisting connection for earthquake resisting structure”, *J. Constr. Steel Res.*, **62**, 295-302.
- Yang, Q. and Yang, N. (2009), “Seismic behaviors of steel moment resisting frames with opening in beam web”, *J. Constr. Steel Res.*, **65**(6), 1323-1336.